

High Resolution Observations of IRAS FSC10214: a $z=2.3$ gravitationally lensed starburst/AGN

R.P. Deane*

University of Oxford

E-mail: roger.deane@astro.ox.ac.uk

S. Rawlings

University of Oxford

E-mail: sr@astro.ox.ac.uk

I. Heywood

University of Oxford

E-mail: ianh@astro.ox.ac.uk

H.-R. Klöckner

University of Oxford, Max-Planck-Institut für Radioastronomie

E-mail: hrk@astro.ox.ac.uk

K. Grainge

University of Cambridge

E-mail: kjbgl@mrao.cam.ac.uk

We present new radio data of IRAS FSC10214, a gravitationally lensed starburst/AGN composite galaxy at $z=2.3$. Our Bayesian MCMC source plane reconstruction places what we argue to be the AGN core (VLA 8 GHz) and the scattered quasar light (*HST* rest-frame ultraviolet) at an angle perpendicular to the ultraviolet polarisation angle. The size of and projected distance to the dominant *HST* UV emission component is roughly consistent with the smooth polarisation angle variation observed with *HST* polarimetry, suggesting that the modelled offset between these two components is reasonably accurate. Both of these components lie inside a larger 1.6 GHz component (observed with *MERLIN*) thought to be dominated by a radio lobe based on its steep radio spectrum but very likely to include star formation as well given the substantial molecular mass ($M_{\text{H}_2} \sim 10^{12} \mu^{-1} M_{\odot}$) in this system. Our lens model finds the *HST* rest-frame UV component is preferentially magnified due to its closer proximity to the cusp of the caustic. A preferential magnification of the narrow line region dust clouds, where the ultraviolet scattering is assumed to occur, supports previous claims that differential magnification could mask the expected polycyclic aromatic hydrocarbon spectral features in the Spitzer mid-infrared spectrum which broadly trace the star forming regions. Further predictions will be tested with upcoming *EVN* and *VLBA* observations.

10th European VLBI Network Symposium and EVN Users Meeting: VLBI and the new generation of radio arrays

September 20-24, 2010

Manchester UK

*Speaker.

1. Introduction

It is now known that star formation and the growth of super-massive black holes in galaxies are strongly linked (e.g. [1]; [2]), however the mechanisms involved are not yet clearly understood. Detailed observations of galaxies at cosmological distances are required to advance our theoretical and subsequent numerical models of galaxy evolution over cosmic time. High spatial resolution observations of galaxies with both starburst and AGN characteristics are able to give a unique perspective of the interplay of these components. This is a particularly powerful probe of galaxy evolution at $z \sim 2$, corresponding to the peak of quasar and star formation activity ([3],[4]). To this end, many observations target gravitationally lensed sources which undergo a natural boost in flux and angular extent. One of the challenges of using this ‘cosmic telescope’ is differential lensing: different emission scales have differing magnification factors that can distort the global SED. This contribution presents first results of an extensive radio/mm observing programme to quantify this effect and the intrinsic SB/AGN energy contributions in the famous strongly lensed system IRAS FSC10214+47 (IRAS 10214 hereafter).

2. Observations

New observations have included *MERLIN* 1.6 GHz, VLA 8 GHz A-array (both resolved) and *GMRT* 330 MHz, Arcminute Microkelvin Imager (*AMI*) 16 GHz (both unresolved). The multi-wavelength study of the object from radio to X-ray is detailed in Deane et al. (2011, in prep.). Here we show the new radio SED data points added in the spectrum and then focus our attention on the resolved maps and inferred source plane structure. As the *apparent* global SED in Fig. 1 illustrates, IRAS 10214 is an obscured AGN with significant star formation, both of which are confirmed by spectral features including a polarised ($>20\%$), broad ($\sim 6000 \text{ km s}^{-1}$) C IV line [5] and a vast reservoir of molecular hydrogen ($\text{H}_2 \sim 5 \cdot 10^{11} \mu^{-1} M_\odot$, [7], [8]). There is substantial mid- to far-infrared dust emission ($M_{\text{dust}} \sim 10^9 \mu^{-1} M_\odot$), strong NIR emission with a steep downward slope toward shorter wavelengths which suggests high extinction by a dusty nuclear torus and/or the host galaxy. Curiously, Spitzer NIR spectroscopy revealed a $9.7 \mu\text{m}$ silicate emission feature [6] which is, naively, not expected in type-II quasars. The host galaxy appears to dominate in the optical band (rest-frame) while the low S/N X-ray detections by both Chandra and XMM-Newton are roughly consistent with the NIR derived luminosity of the buried AGN (with column density $N_{\text{H}} > 10^{23} \text{ cm}^{-2}$; [17]). The (sub)millimetre observations reveal a substantial dust mass, while line observations in this part of the spectrum have measured high molecular masses (low to high J CO, HCN, C I; e.g. [7]).

We have extended the radio SED coverage which confirms a steep spectrum component ($\alpha = 1.0$, where $\alpha \equiv -\frac{\log(S_1/S_2)}{\log(\nu_1/\nu_2)}$) between $\nu_{\text{obs}} \sim 330 \text{ MHz}$ to 4.8 GHz. The spectrum flattens between 4.8 GHz and 16 GHz with an apparent peak at 8 GHz, most likely as a result of a flat-spectrum AGN core. Our two high resolution radio maps trace both these regions, while the *HST* 814W map of [9] is dominated by scattered quasar light as inferred from *HST* polarisation observations and suggested by the SED. The larger, 1.6 GHz component (observed with *MERLIN*) is thought to be dominated by a radio lobe based on its steep radio spectrum but likely to include star formation as well given the substantial molecular mass ($M_{\text{H}_2} \sim 10^{12} \mu^{-1} M_\odot$). In subsequent modelling, we

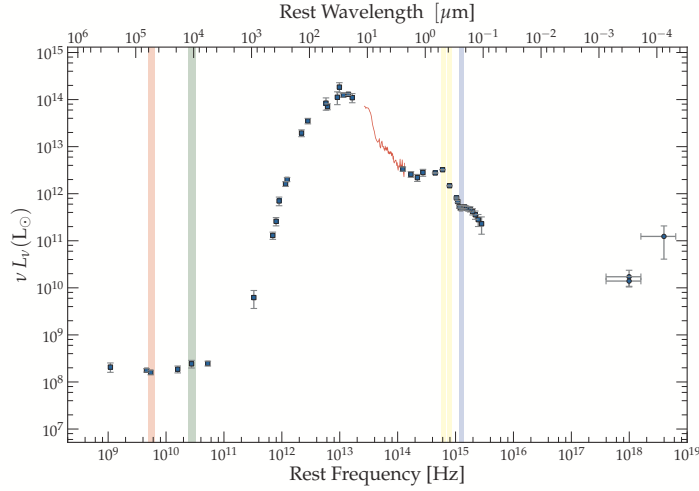


Figure 1: The X-ray through radio SED of IRAS FSC10214 showing the three bands probed by the high resolution imaging presented in this work: radio jet (blue), AGN core (red), scattered quasar light (green) as traced by the *MERLIN* 1.6 GHz, *VLA* 8 GHz and *HST* WFPC2 instruments respectively. Yellow bands represent the *HST* NICMOS 1.1 μm and 1.6 μm imaging which trace the host galaxy’s stellar component.

assume the 1.6 GHz, 8 GHz and HST814W maps are dominated by the lobe, core and scattered quasar light respectively.

2.1 *MERLIN* 1.6 GHz

IRAS 10214 was observed for 24 hours with *MERLIN* array including the 76 metre Lovell Telescope. J 1027+480 was used as a phase calibrator ($\Delta\theta \sim 1^\circ$) and B 2134+004 was used as a pointing calibrator (positional accuracy < 0.36 mas). We achieve a $1\text{-}\sigma$ noise sensitivity of $\sim 45 \mu\text{Jy}$ per 405×349 mas² beam. The resultant map reveals a resolved ‘arc’ (Fig. 2, left panel) roughly co-spatial with the HST814W image [9]. A number of 2-3 σ peaks are seen in the region of the foreground lensing galaxy as well as the counter-image position as reported by [9], however nothing further can reliably be inferred at this low significance. A comparison of the *uv*-tapered and full resolution maps suggests that no flux is resolved out. The 330 MHz through 4.8 GHz spectral index suggests, within the errors, that no significant extended flux is resolved out in the *MERLIN* 1.6 GHz map.

2.2 *VLA* A-array 8 GHz

IRAS 10214 was observed twice with the *VLA* in X-band in the 1990s, both with consistent flux densities and centroid positions. The second, deeper observation achieved a sensitivity of $13 \mu\text{Jy beam}^{-1}$. Both sets of data have been re-reduced and combined to produce the map in Fig. 2 (middle panel). Independent astrometry shows a spatial offset between the dominant peak and the *HST* optical peak of ~ 0.4 arcsec. This offset is consistent with the much shallower X-band observation by [10] who measured an offset of $\Delta\theta = 0.63 \pm 0.37''$. Apart from the main detection of the ‘arc’, the combined 1991/1995 map reveals two $4\text{-}\sigma$ peaks, one eastward of the ‘arc’, the other eastward of the optical counter-image. The latter has a very low arc/‘counter-image’ ratio $\tilde{\mu} =$

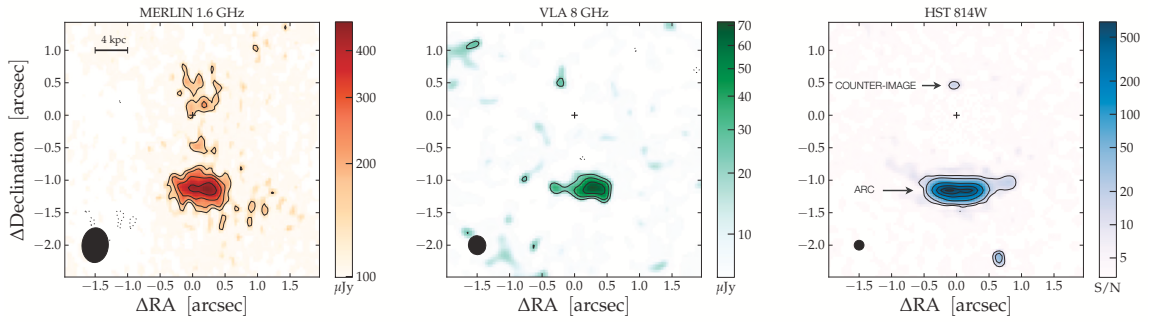


Figure 2: **Left panel:** MERLIN 1.6 GHz map with $\sigma \sim 46 \mu\text{Jy}$ per $405 \times 349 \text{ mas}^2$ beam. **Middle panel:** 8 GHz VLA map with $\sigma \sim 11 \mu\text{Jy}$ per $292 \times 267 \text{ mas}^2$ beam. **Right panel:** HST814W map with counter-image and arc. The integrated arc/counter-image flux density ratio is $\bar{\mu} \sim 75 \pm 25$. Note that the lens has been fit using GALFIT and removed from this image. The FWHM of all PSFs are shown in the lower left of each frame. The cross indicates the centroid of lensing galaxy as measured from the HST160W map.

8, inconsistent with all previous and the current study’s lensing results. This radio ‘counter-image’ is not seen in either of the 1991 and 1995 maps and so despite its $4\text{-}\sigma$ significance this is not a robust feature. We therefore assume the detection is *not* secure.

2.3 HST814W

IRAS 10214 was observed with the WFPC2 F814W filter during two orbits on 10 December 1994. The morphology (see Fig. 2, right panel) shows a clear $\sim 1''$ long arc and a low S/N detection of the counter-image. The observations, derived properties and lens modelling are fully described in [9]. Two key attributes of this map are accurate PSF characterisation and astrometry. The PSF FWHM is $\sim 100 \text{ mas}$ as derived from the ‘Tiny Tim’ *HST* software package using a *K*-star source colour since an accurate empirical estimate was not possible. This is fully described in [9] and is consistent with two stars in the field, one of which is saturated and the other too weak for accurate PSF estimation. The astrometry is in agreement with determinations from [12, 9, 14] and Simpson et al. (2011, in prep) to within $\Delta\theta < 10 \text{ mas}$.

3. Lens Model

The leading lensing model in the literature of IRAS 10214 is that derived by [9]. They use a least-squared approach, minimising the distance between the model and the 96 brightest pixels in the arc and the brightest pixel in the counter-image. Their modelling found an isothermal sphere ellipticity of $q = 0.3$, position angle $PA = -11^\circ$, and Einstein radius $\theta_E = 0.82''$ to match the arc/counter-image ratio of $\sim 50 - 100$ in the HST814W map. We have written a Bayesian MCMC algorithm to determine a new lens model and quantify the associated uncertainties. We select observationally motivated priors based on the position angle and ellipticity of the deep, unpublished *HST H*-band map. There are two major advantages to this: **(1) Sensitivity:** the HST 160W map has roughly a factor of 2 better S/N than the HST814W map. **(2) Dark Matter Tracer:** the lensing galaxy is observed at rest-frame *R*-band tracing the older, more virialised stellar population which

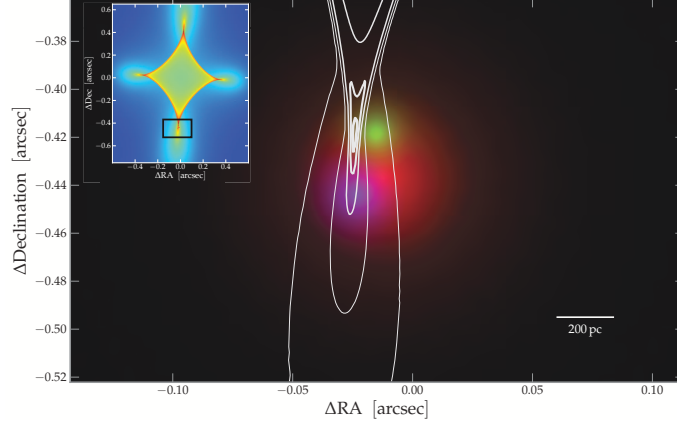


Figure 3: IRAS 10214 Source plane reconstruction showing the AGN core (green), scattered quasar light (blue), and radio lobe (red). White contours represent lines of equal magnification at $\mu = 10, 20, 50, 100, 150$.

will better sample the dark matter potential. We derive the position angle and ellipticity priors of the lensing galaxy from 10^4 GALFIT two-dimensional Sersic fits to the HST160W data, performed in Monte Carlo sense, varying all initial values. The MCMC derived lens model parameters are: ellipticity $q = 0.2 \pm 0.02$; position angle $PA = -4^\circ \pm 3^\circ$; Einstein radius $\theta_E = 0.865 \pm 0.03''$ which is the equivalent of a one dimensional velocity dispersion $\sigma_v = 255.5 \text{ km s}^{-1}$ for an isothermal dark matter halo distribution. The full lens model derivation is detailed in Deane et al. (2011, in prep).

4. Results

The derived 2D marginalised posterior probability distribution functions of the source plane parameters show that the position and radii of each component are tightly constrained. The confidence levels show a high degree of statistical evidence that these components have offset centroids. As expected in our simple model (of radio lobe, core and scattered light), the core component, presumed to dominate the 8 GHz map, has the smallest source plane scale radius ($r_s = 17$ mas, 138 pc at $z = 2.3$). This yields a magnification of $\mu = 16$. The source size expected from a GPS source which peaks at ~ 25 GHz is 50 pc [13], broadly consistent with the core scale radius of 138 pc derived here. The *HST* source plane model scale radius ($r_{814} = 23$ mas) is larger than derived in [9] ($r_{814, E1596} \sim 5.5\text{-}10$ mas), due to the lower magnification of $\mu = 35$ (cf. $\sim 50\text{-}100$ in [9]). It appears that all previous work on IRAS 10214 has approximated the magnification with the arc to counter-image ratio. This is found to be incorrect by factors 3-4 for the three maps investigated here. For example, the HST814W best fit model has an arc to counter-image flux ratio $\check{\mu} = 92$, however the true magnification (image to source plane flux ratio) is $\mu = 35$. The radio lobe presumed to dominate the 1.6 GHz map is fit with an intrinsic scale radius $r_s = 58$ mas (~ 480 pc), the largest of the three components. The magnification is $\mu = 18$. Systematics dominate the error budget in these lensing results, particularly the choice of an singular isothermal ellipsoid (inner density slope $m = -1$), which contributes a $\sim 20\%$ error based on the SLACS results.

5. Current View

Our source plane reconstruction (Fig. 3) yields an intrinsic structure consistent with a number of previous observations. These include: **(1)** the radio axis is roughly perpendicular to the UV polarisation position angle ($PA = 62^\circ \pm 3^\circ$ east of north). This utilises the analytical result that the polarisation angle is unaffected by lensing [15]. **(2)** The distance between scattered light and the core ($\Delta R \sim 300$ pc) is roughly consistent with the smooth polarisation angle variation measurement by *HST* [12]. Clouds of a finite size scatter photons from a continuum point source perpendicular to the angle of incidence. Therefore, if the scattering cloud source size (R_{source}) is known, along with the maximum change in polarisation angle ($\Delta\theta_{\text{max}}$), then the distance to the AGN (R_{dist}) can be estimated with the simple relation $d_{\text{AGN}} \sim \frac{R_{\text{source}}}{\Delta\theta_{\text{max}}} = 420$ pc assuming $R_{\text{source}} =$ twice the scale radius. This compares favourably with the independently derived $R_{\text{dist}} = 220$ pc in our source plane reconstruction. Astrometric shifts of 100 mas (*VLA /MERLIN* absolute astrometric accuracy) show $< 25\%$ changes in source radius and the 8GHz-*HST*814W source plane separation, demonstrating that astrometric error is not the cause of these modelled offsets.

6. Conclusions and Future Observations

We report a new lens model for IRAS 10214 with robust uncertainty estimates. We find the arc to counter-image flux ratio is a poor estimate of the magnification and hence derive a significantly lower magnification for this galaxy. We also find the *HST*814W, likely emanating from the narrow line region is preferentially magnified by a factor > 2 . The source plane structure suggested here will be immediately tested by upcoming *EVN* and *VLBA* observations at 1.6 GHz and 330 MHz respectively. The combination of these observations with the dual-frequency VLBI data will allow us to make significant progress toward disentangling the co-existence of a starburst and active nucleus in a galaxy observed at the peak epoch of these two fundamental galaxy evolution mechanisms.

References

- [1] Magorrian, J. et al., 1998, *AJ*, 115, 2285
- [2] Ferrarese, L. and D. Merritt, 2000, *ApJ*, 539, L9
- [3] Dunlop, J. S. and J. A. Peacock, 1990, *MNRAS*, 247, 19
- [4] Madau, P. et al., 1996, *MNRAS*, 283, 1388
- [5] Goodrich, R. W. et al., 1996, *ApJ*, 456, L9
- [6] Teplitz, H. I. et al., 2006, *ApJ*, 638, L1
- [7] Ao, Y. et al., 2008, *A&A*, 491, 747
- [8] Solomon, P. M., S. J. E. Radford, and D. Downes, 1992, *Nature*, 356, 318
- [9] Eisenhardt, P. R. et al., 1996, *ApJ*, 461, 72
- [10] Lawrence A., et al., 1993, *MNRAS*, 260, 28
- [11] Koopmans, L. V. E. et al., 2006, *ApJ*, 649, 599
- [12] Nguyen, H. T. et al., 1999, *AJ*, 117, 671
- [13] O’Dea, C. P., 1998, *PASP*, 110, 493
- [14] Evans, A. S. et al., 1999, *ApJ*, 518, 145
- [15] Dyer, C. C. and E. G. Shaver, 1992, *ApJ*, 390, L5
- [16] Simpson, C. et al., 2010, in prep.
- [17] Alexander, D. M. et al., 2005, *MNRAS*, 357, L16